Spherical depth-sensing nanoindentation of human anterior skull base bones: Establishment of a test protocol

Valentin Favier, Patrice Gallet, Olivier Ferry, Jean-Philippe Jehl

Title: Spherical depth-sensing nanoindentation of human anterior skull base bones: establishment of a test protocol

Authors: Valentin Favier[1,2], Patrice Gallet[3], Olivier Ferry[4], and Jean-Philippe Jehl[5]

1 Aide à la Décision pour une Médicale Personnalisée, EA2415, Département MIPS, Université de Montpellier, Montpellier, France;

2 Département d'ORL et chirurgie cervico-faciale, Centre Hospitalier Universitaire de Montpellier, Montpellier, France;

3 Département d'ORL et chirurgie cervico-faciale, Hôpital Brabois, CHRU Nancy, Université de Lorraine, Vandoeuvre-lès-Nancy, France;

4 Institut Jean Lamour – Centre de compétences Xj – CNRS UMR 7198, Université de Lorraine, Nancy, France;

5 Institut Jean Lamour – CNRS UMR 7198, Université de Lorraine, Nancy, France

Corresponding author e-mail / address

Dr Valentin Favier

Department of Otolaryngology-Head and Neck Surgery, Gui de Chauliac Hospital, University Hospital of Montpellier, 80 Avenue Augustin Fliche, Montpellier 34000, France

Tel.: +33 (0)4 6733 6803, Fax: +33 (0)4 6733 6808

E-mail: valentin_favier@hotmail.com

ORCID: 0000-0002-7999-951X

Abstract

The mechanical properties of anterior skull base (ASB) bones are not well understood due to their complex geometry and deep location. However, it is of particular interest for skull base surgeons to appraise the force range they can apply during procedures and know what kind of haptic feedback a simulation device should produce in order to be realistic for trainees. The aim of this study was to establish a measurement protocol to set the level of hydration state, temperature and curve analysis method for spherical depth sensing nanoindentation of ASB bones. A definitive screening design method was used to test the different possible combinations of these factors. Two samples of ASB bones from the heads of two human body donors (two specimens) were selected according to their microstructure as assessed by micro-CT (microtomography): low-porosity (16.87%, sphenoid bone) and high-porosity (79.85%, ethmoid bone). Depth measurement series of 36 nanoindentations (n=288) were performed on specimen 1 according to the L8 Taguchi orthogonal array to study the effect of temperature (two levels: 20 or 37°C), hydration state (dry or immerged in physiological saline sodium chloride), and loading curve analysis according to the Hertzian contact theory (fitting at the start or at the end). The mean values of reduced Young's (E*) modulus varied significantly depending on the hydration status and bone microstructure. In order to obtain the physiological properties of ASB bones, we thus propose performing immersion tests. To simplify the experimentation protocol, future experiments must include a room temperature level and a fit of the curve at the end of the load. A validation series was performed on the second specimen to assess the set of parameters. The E* in dry bone gave mean values of 994.68 MPa, versus 409.79 MPa in immerged bones ($p < 0.00001$). This is the first time a study has been carried out on ASB bones, defining the experimental parameters related to physiological conditions.

Keywords: Anterior skull base, bone, spherical depth sensing nanoindentation, temperature, hydration, experimental design, mechanical properties

1. Introduction

Anterior skull base (ASB) bones, comprising the frontal, ethmoid, and sphenoid bones, must be partially broken and resected in many endoscopic endonasal skull-base operations to access tumor or inflammatory lesions. These bone structures are close to vital anatomical structures, such as the internal carotid arteries, brain, and optic nerves (Hosemann and Draf, 2013). Therefore, an understanding of their mechanical properties may help surgeons analyze and prevent surgical complications, such as uneventful perforation of the ethmoid roof (White *et al*., 2004). It could also be useful to understand what type of haptic feedback a simulation device should give to be realistic for trainees (Favier *et al*., 2019).

Most biomechanical studies on skull bones report on the behavior of the calvaria, which protects the brain from external injuries, to understand the mechanisms of skull fractures in forensics (Raul *et al*., 2008) and traumatology (Alexandre *et al*., 2019). In this perspective, authors have studied the whole bone without distinguishing between cortical and trabecular bone to better understand the mechanisms of skull fractures. The ASB bones, located at the interface between the brain and paranasal sinuses, are of particular interest because of their unusual anatomy, which has no equivalent anywhere in the body. They comprise sections featuring thin bone walls (approximately 100 micrometers' thick) that encompass the paranasal sinuses and are mainly cortical in nature, with no or little trabecular bone (Berger *et al*., 2013). Due to this unique, complex, and variable anatomy (see geometry, Figure 1), it is impossible to collect standardized specimens to perform common material tests. Therefore, to test the mechanical properties of ASB bones one must consider the microstructure rather than the macroscopic geometry of bone samples. Spherical depth-sensing nanoindentation is a localized test that studies mechanical properties at the tissue level, related to a microscopic structure. It has never before been used to characterize ASB bones. According to a study by Rodriguez-Florez (Rodriguez-Florez *et al*., 2013), the tissue-level mechanical properties of bone

79 measured by nanoindentation depends on the hydration state and data analysis method, among
80 other factors.

81 Thus, the optimal parameters for studying ASB bones using nanoindentation are unknown. According
82 to our previous experiment in sampling thin walls of ASB bones (Favier *et al*., 2017), the consistency
83 of ASB bones seems to be affected by the hydration state: the more exposed to ambient air the
84 samples were, the more brittle they became. Other parameters may interfere with the results of
85 experiments. For example, samples are usually at room temperature (20°C) during tests, while the
86 body temperature is 37°C. Different analysis methods on loading curves may also influence the final
87 value of the reduced Young's modulus (E*) (Fischer-Cripps, 2001). This modulus is a characteristic
88 that can define the localized mechanical behavior of a material. Subsequently, using this E* is a way
89 to compare different structures of bones.

90 An experimental design was carried out i) to evaluate and define the level of experimental
91 parameters (temperature, hydration and curve analysis) influencing the nanoindentation tests of ASB
92 bones and ii) to analyze the interactions or dependencies between these variables (factors).

93

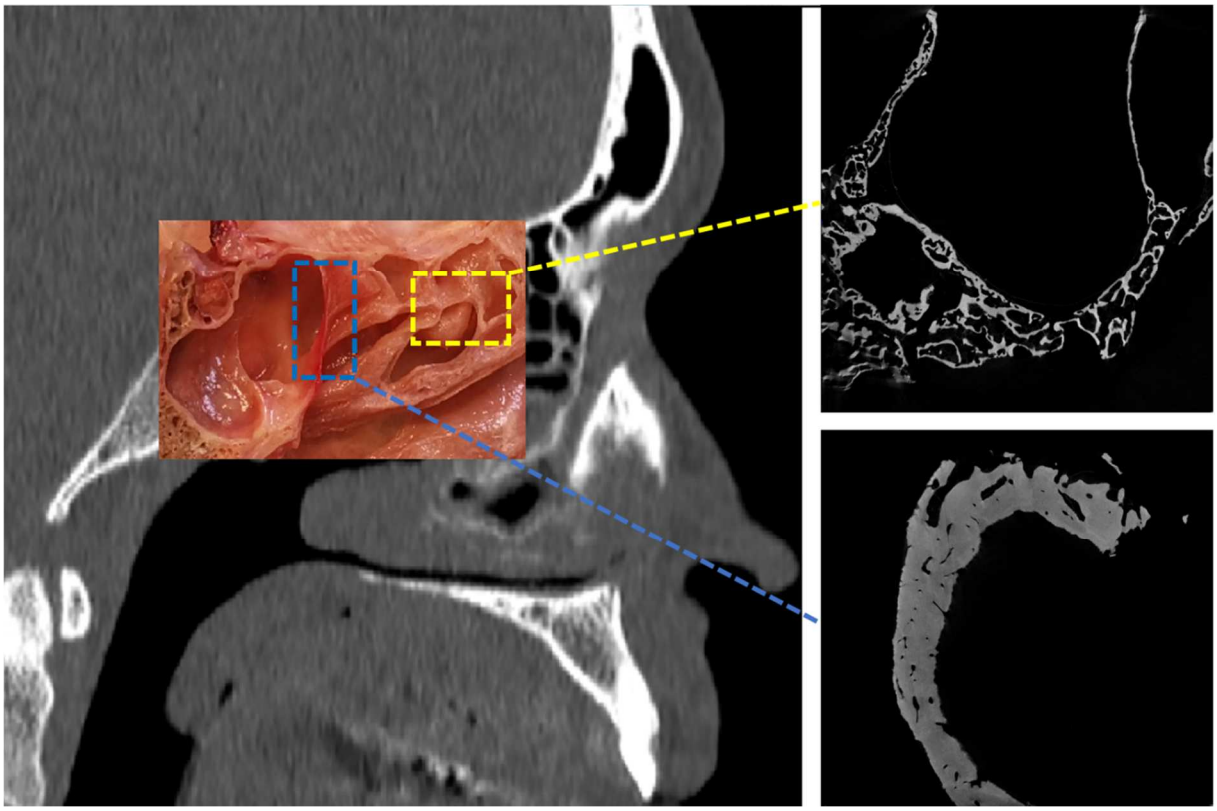

Figure 1: Sample extract sites and micro-CT imaging (Specimen 1). Yellow: ethmoid bone (high-porosity level shown in micro-CT), acquisition with 5 µm voxel size; blue: sphenoid bone (low-porosity level in micro-CT), acquisition with 3.75 µm voxel size

2. Material and methods

2.1 ASB samples

The samples were extracted from two human heads (two men, 81 and 84 years-old, without known disease related to their skeleton), each from bodies donated to the anatomy laboratory of Nancy, France.

Each head was preserved frozen at -18°C, without any chemical fixation. For the sampling, the head underwent parasagittal hemisection, and two samples were meticulously extracted from the left side: one from the ethmoid cell walls and one from the anterior wall of the sphenoid sinus (Figure 1). Each bone sample was separated from its surrounding mucosa and periosteum.

In order to avoid the samples deteriorating, they were immediately refrozen following a common procedure (Bakhach et al., 2009, Dall'Ara *et al*., 2012) for bone samples conservation. The samples were not stored in saline, but frozen without medium, just after extraction from the heads. All samples were stored in airtight boxes.

The indent area of 1 mm² was selected without visible porosity using the microscope integrated in the system (Rho *et al.*, 1997). A roughness test (Taylor-Hobson, Leicester, United Kingdom) was then performed on this surface. The surface was eligible for nanoindentation when the local roughness defect (Rt) was less than or equal to 0.02 µm for a sampling length (Lc) of 250 µm. Before the test, the sample was placed on a sample holder (Petri dish), and fixed with cyanoacrylate and sand grains allowing the adjustment of the horizontality of the surface to be indented (by microscopy integrated in the system). This made it possible to obtain perpendicularity between the tested surface and the axis of the indenter.

2.2 Micro-CT imaging

Each sample was scanned using X-ray micro-CT (microtomography) (Figure 1) with the Nanotom S Phoenix X-ray (Baker Hughes GE, Boston, Massachusetts, USA, 180 kV - 150 µA, 25 W) at maximum accuracy according to the size of the sample. Before starting experiments, a blank of detector noise was recorded, then subtracted of radiography data set. Samples were placed frozen in the micro-CT to be thawed in ambient air atmosphere (constant temperature during micro-CT acquisition, approximately 20°C) and put on a polyethylene rod holder with a polystyrene home-made holder stuck on it, to avoid samples movement during the acquisition process. Scanning in air affords the highest contrast between the specimen and surrounding medium (Bouxsein *et al.*, 2010). Total scan time was 144 minutes per sample (0.25° step, 1440 images, 6 second exposure, 80 KVp, 6.5W, microfocus beam 2 µm). The distance between the detector and the source was set to 200 mm and sample-source distance was set to 20 mm, with a constant magnification factor of 13.3. No dilatation

was observed during experiments. Voxel size was 3.75 µm in each dimension (isometric) for "low-porosity" bone (LPB) and 5 µm for "high-porosity" bone (HPB). For 3D-imaging reconstruction, the cone-beam algorithm of Feldkamp was applied using Phoenix datos|x software (GE, Boston, Massachusetts, USA). The 3D qualitative representation of the porosity (LPB or HPB, see Figure 1) was obtained by importing the ".raw" file (16 bits) in the 3D software (VGStudio Max 3.3 material package, Volume graphics, Heidelberg, Germany). To accurately distinguish voids from bone material, some filters were applied (adaptive gauss and opacity mapping filters) on each volume. Finally, the porosity was calculated as the total pore volume divided by the total sample volume (Boughton et al., 2019), using the porosity analysis VGDefX algorithm of VGStudio Max. Porosity rate (obtained from bone volume fraction, BV/TV) and wall thickness were calculated directly from the numerical model of the specimen (Bouxsein *et al.*, 2010).

2.3 Spherical depth-sensing nanoindentation

An ultra nanoindenter (UNHT^3 Bio) from ANTON-PAAR, Peseux, Switzerland (Figure 2) was used. This system enables testing at penetration depths varying from just a few nanometers to 100 µm, using loads of up to 20 mN. The depth resolution was 0.006 nm and the load resolution 0.001 µN. The radius of the spherical indenter (diamond tip) was 100µm. The contact surface disc generated by indentations did not exceed a radius of 30 µm. The load and unload speeds were intentionally kept low (40 mN/min), enabling us to generate bone elasticity as well as reversible deformations, avoiding any interference from neighboring indentations. The tool was adapted to enable testing on biological materials in liquid medium. Raw data curves were obtained using OriginPro 9 software (OriginLab, Northampton, Massachusetts, USA).

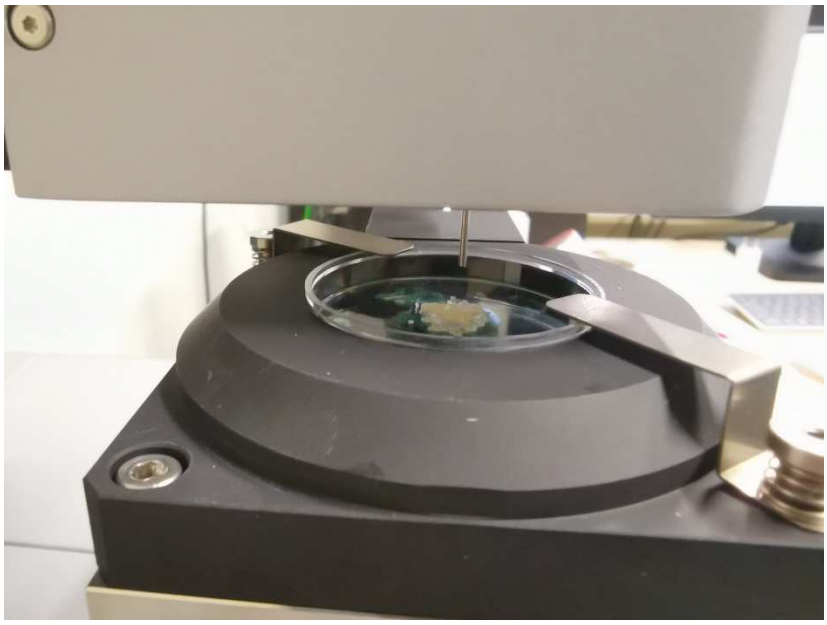

Figure 2: Bone samples placed in the Anton Paar ultra nanoindenter (dense bone, dry environment)

2.4 Experimental design

Due to the nature of ASB bones (different microstructures and organizations), how the environmental factors of the test and their inter-factor interactions influenced the results should be assessed in order to define the optimal test configuration. The following parameters were studied: temperature (two levels: 20°C; 37°C) and hydration (two levels: testing in liquid environment with physiological saline sodium chloride after one hour of immersion; in ambient air). To ensure this protocol would be usable for all bone structures, we introduced two “extreme” bone microstructures: one LPB, the other HPB (Figure 1). Furthermore, we studied two analysis methods for characterizing bone structures: one where the loading curve was fitted at the start, the other applying it at the end, to separate any influence of potential residual soft tissues (periosteum) or surface irregularities.

One way of addressing this issue of fixed parameters is to conduct an experimental approach testing the different possible combinations of these factors. We used the "definitive screening design" method according to the following principles (Lundstedt *et al*., 1998).

Consider an experiment of which the outcome depends on *p* parameters. Assume that the range of variations of each parameter can be subdivided into *n* levels. The basic experimental design requires p^n experiments. This is evidently not a feasible approach for problems that depend on a high number of parameters, however, such as those encountered in living organisms. In order to overcome this obstacle, one should use the fractional factorial designs introduced by Genichi Taguchi (Taguchi, 1990]). Then, one can perform a simplified analysis of interactions and evaluate the impact of each parameter.

Each sample was defrosted at room temperature (20°C) for the micro-CT acquisition and fixed to a support with glue before being tested with the nanoindenter. A series of 36 indentations was performed for each step of the experimental design, using the same load on each sample analyzed. According to an L8 Taguchi orthogonal array (Taguchi, 1990), a total of eight series were performed to analyze all the parameters mentioned above (*i.e.,* 288 indentations, Table 1).

Tests	Bone microstructure	Hydration status	Temperature	Analysis
# 1	Low-porosity	Dry	20°C	Start
# 2	Low-porosity	Dry	37°C	End
# 3	Low-porosity	Hydrated	20°C	End
# 4	Low-porosity	Hydrated	37°C	Start
# 5	High-porosity	Dry	20°C	End
# 6	High-porosity	Dry	37°C	Start
# 7	High-porosity	Hydrated	20°C	Start
# 8	High-porosity	Hydrated	37°C	End

Table 1: L8 Taguchi orthogonal array for indentation tests configuration

2.5 Data analysis

Bone tissue has a viscoelastic behavior. In this study, we focused only on its elastic behavior thanks to low speed loading (quasi-static) and low load (low displacement). It is thus possible that, at very shallow indenter penetration depths, the surface of contact between the sample and indenter takes a similar form to a disc. Given these properties, one can apply an analysis of elastic contact (Jehl *et al.*, 2016). Thus, a strategy enabling to define the range of values on commencing the load was designed, for which the Hertzian contact relation (Hertz, 1882) can be applied. As a brief reminder, this formula establishes the relationship between the force applied (F), the relative approach distance between the two elements (h), and the radius of the disc contact area (a) (formulae (1) and (2)). These formulae also implicate the radius of the indenter's curve (R) and the mechanical characteristics of the sample and indenter, *i.e.* their Young's moduli and Poisson's ratios, using the reduced elasticity modulus, defined by formula (3).

$$h^3 = \left(\frac{9.F^2}{16 \times R \times E^{*2}}\right) \quad (1)$$

$$a = (R \times h)^{1/2} \quad (2)$$

$$\frac{1}{E*} = \frac{1-\nu^2}{E} + \frac{1-\nu_p^2}{E_p} \quad (3)$$

In formula (3), E_p and ν_p represent, respectively, the Young's modulus and Poisson's ratio of the indenter. When the rigidity modulus of the tested material is very weak compared to that of the indenter, it is calculated as $E^* = E/(1-\nu^2)$.

During the indentation testing, the penetration depth was continually recorded according to the applied load. After each test, a series of data pairs (F, h) was generated, from which one would be able to identify the characteristics of the material tested using formula (1). In log-log plotting, this formula becomes:

$$\ln(F) = \frac{3.\ln(h)}{2} + \frac{1}{2}\ln(\frac{9}{16.R.E^{*2}}) \qquad (4)$$

The aim was thus to identify the parameters of a linear function.

Figure 3 presents a test on a calibration sample: the determination of the contact point (Figure 3A) allows shifting the origin of the loading curve (Figure 3B). The reduced Young's modulus (E*) was calculated both at the start and end of the loading curve to evaluate the influence of data analysis on measurement. The fittings produced similar scores (E*). Thus, there was no significant difference between the two fittings, but the "end" part of the curve provided a better fit of the slope for the reduced Young's modulus calculation (R=1 for all tests), since surface irregularities have less effect.

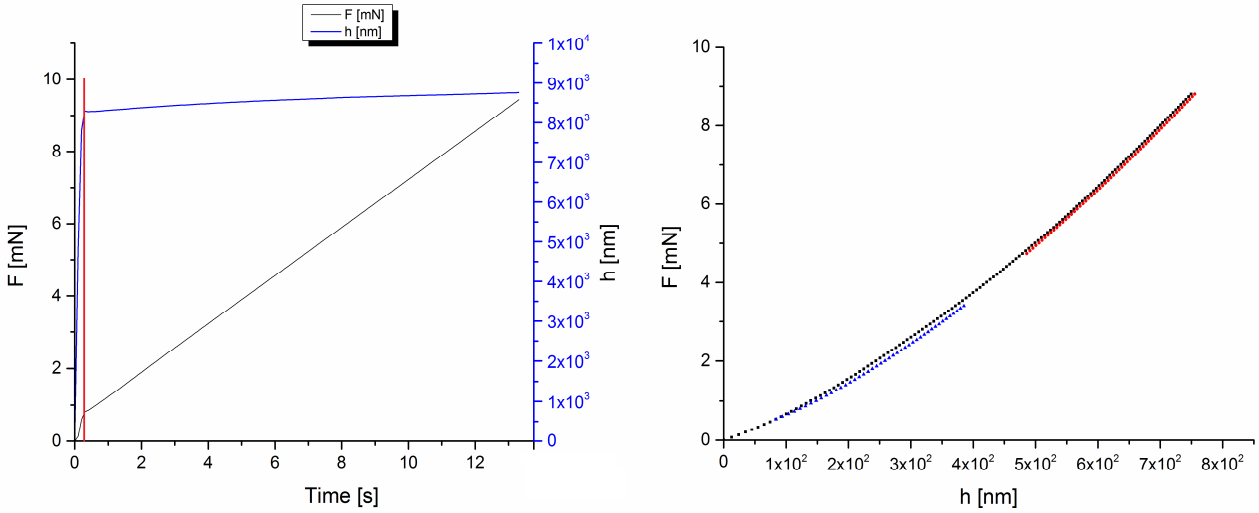

227

228 *Figure 3: A: Graphical determination of the contact point (red line) from the curves h(t) and F(t). B:*

229 *Comparison of curve analysis on a calibration sample. Black dots: loading curve; blue dots: fit at the*

230 *start of the curve; red dots: fit at the end of the curve*

231

232 2.6 Ethical considerations

233 This study is in accordance with the Helsinki Convention (1964), the French legislation governing the

234 donation of bodies and the relevant guidelines and regulations from the laboratory of anatomy of

235 Nancy, France. Neither donor was from a vulnerable population, and written informed consent was

236 obtained for all anatomical and surgical studies.

237

3. Results

Bone volume fraction was 20.15 % (porosity of 79.85 %) on HPB and 83.13% % (porosity of 16.87%) on LPB. The minimum thickness of the indented zone was 48 µm for HPB and 105 µm for LPB.

The main results are summarized in Table 2 and categorized by the four parameters of analysis: density of bones, hydration of the environment, temperature of samples, curve analysis. Figure 4 presents a box-plot graph illustrating the mean values and dispersion of E* according to the different parameters.

Characterization	Reduced Young's Modulus E* (mean)	**Reduced Young's Modulus E* (median)**	Standard deviation E*	**Range**	P-value (test)
Low-Porosity Bone	519.66 MPa	491.23 MPa	182.82 MPa	157.61 to 934.08 MPa	< 0.00001 (Welch's t-test)
High-Porosity Bone	350.68 MPa	351.68 MPa	104.65 MPa	147.42 to 545.33 MPa	
Environment: dry	697.13 MPa	665.56 MPa	221.32 MPa	545.33 to 934.08 MPa	< 0.00001 (Wilcoxon)
Environment: liquid	173.21 MPa	177.34 MPa	66.16 MPa	147.42 to 230.2 MPa	
Temperature: 20°C	419.92 MPa	422.2 MPa	109.88 MPa	147.42 to 756.74 MPa	0.0836249 (Welch's t-test)
Temperature: 37°C	450.42 MPa	420.7 MPa	177.60 MPa	157.59 to 934.08 MPa	
Curve analysis: start	403.54 MPa	401.09 MPa	141.48 MPa	147.42 to 756.74 MPa	0.000285377 (Welch's t-test)
Curve analysis: end	466.80 MPa	441.81 MPa	145.99 MPa	157.59 to 934.08 MPa	

Table 2: Main results of characterization according to studied parameters (Specimen 1)

A statistical comparison was performed using Welch's t-test for normal distribution variables (density, temperature, and curve analysis) due to the unequal variances in the series. The distribution of values in the "temperature: 20°C" record was not normal, so a Wilcoxon test was performed to

compare the effect of porosity on measured mechanical properties. There was no statistical difference between the temperature parameters, yet the bone porosity and environmental factors were found to effect significant changes in the measured mechanical properties. A comparison of the loading curve fitting parameters revealed a statistical difference, although the absolute difference was 63 MPa. On the other hand, hydration seemed to have a huge impact on measured properties, varying by up to 400%. Finally, spherical depth-sensing indentation was proven able to distinguish between different porosity levels, leading to different mechanical properties.

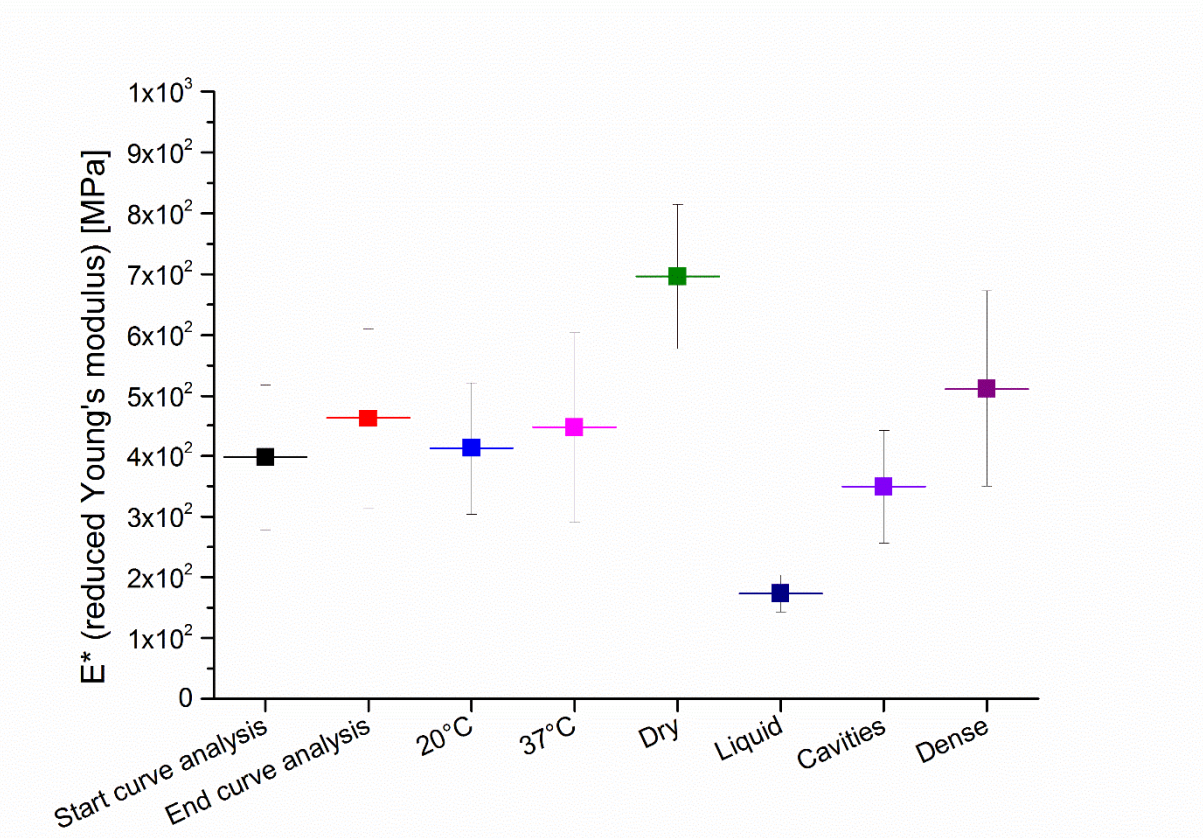

Figure 4: Comparison of in vitro properties of anterior skull base bone following different testing parameters (see L8 Taguchi orthogonal array, Table 1). Means and dispersion of reduced Young's moduli (E) for a series of 36 indentations per sample (288 indentations)*

To complete the analysis of the impact of individual factors, the presence or absence of interactions between these factors should be verified. Three plots (Figure 5) allow this verification. They are "x–y line plots of cell (level combination) means on the response variable for each level of one factor over

all the levels of a second factor" (Lovie, 2005). The title of each plot provides information on the interaction tested. E* is represented on the y-axis. On the x-axis, the two levels of a studied parameter are represented (discrete variable). Thus, if the lines or profiles corresponding to the separate factor levels are parallel, that is, no differential effect over different combinations of the levels of the factors is revealed, then there is no interaction. If they are not parallel, then an interaction is present.

Figure 5A shows a decreasing trend in E* for both bone microstructures (red and blue curves) when the environment changes (dry then liquid). An interaction between bone microstructure and hydration status led to a difference in elasticity between the two bones: greater in a dry environment (approx. 300 MPa) than in a liquid medium (approx. 50 MPa), i.e., a difference of 250 MPa. The slopes of Figures 5.B and 5.C are similar, and the differences are lower than 50 MPa, thus inducing only slight interactions that are negligible.

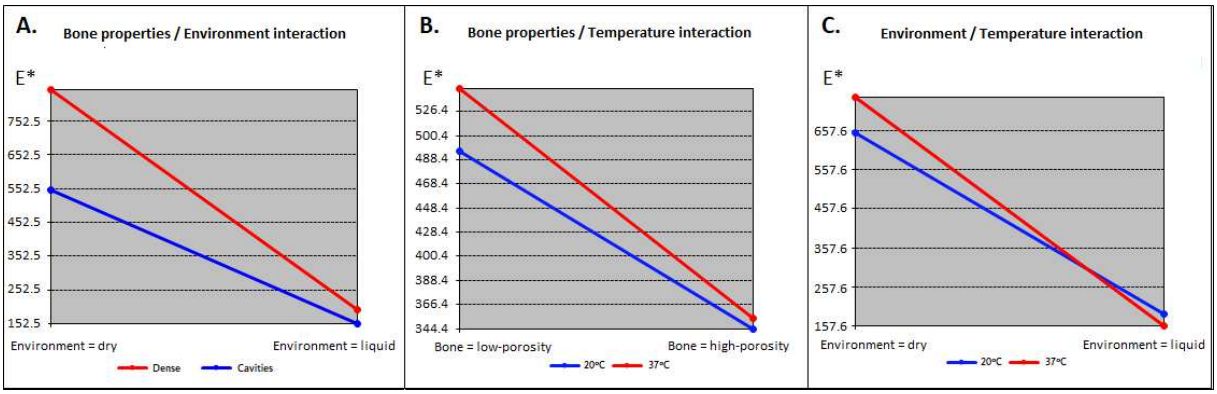

Figure 5: Interaction plot: representation of interactions according to the experimental design method (Lovie, 2005).

4. Discussion

To the best of our knowledge, this is the first study on the mechanical characterization of the thin bone walls of the ASB. Biological tissues are known for their viscoelasticity behavior (Oyen *et al*., 2012). The Hertzian load-displacement relation (Hertz, 1882) focuses on the elastic behavior (quasi-static loading at low load). It was used to define the measurement environment of spherical depth sensing nanoindentation.

Waridel *et al.* studied the stress resistance of ethmoid and sphenoid bones using dynamometer measurement (Waridel *et al*., 1997) to understand the pressure required to cause bone breakage at 11 anatomical sites (bones conserved in 40% ethanol). They identified that highly fragile sites correlated with the location of surgical complications relating to endonasal endoscopic sinus surgery, although did not include characterization of mechanical properties. This finding is of particular interest for Ear Nose and Throat surgeons and neurosurgeons who usually perform endoscopic endonasal surgical procedures. Surgeons need to safely break and remove these walls to access the boundaries of the nasal fossae and sinuses in order to treat infectious diseases or tumors of the ASB. Thus, understanding the mechanical properties of these bones is essential for surgeons at different levels. First of all, it is important for a better design of surgical simulators. Indeed, surgical simulators (i.e., virtual simulator with haptic feedback and/or physical simulators) have to replicate the complex anatomy and mechanical properties of ASB bones. This is, of course, important for improving the visual and haptic realism of the simulation, but also mandatory for safety reasons. Ethmoid and sphenoid bones are surrounded by vital structures such as the forebrain, orbits, optic nerves and internal carotid arteries. By practicing with a simulator with inadequate feedback, trainees could learn to apply aberrant and potentially dangerous forces in the operating room (Yamauchi et al., 2002). Furthermore, it could induce negative training transfer (Våpenstad et al., 2017). Second, these data are required for the objective assessment of these simulators. Currently, the “mechanical fidelity” of simulators is only assessed by subjective ratings provided by users, as there are no data

on the mechanical behavior of these bones. Through biomechanical characterization, simulators may be more "realistic", by selecting appropriate materials (Favier *et al.*, 2017) or improving haptic feedback (Favier *et al.*, 2019). Third, biomechanical data may help design surgical robots by appraising the range of forces that an automated device may apply on these structures. Finally, knowing mechanical properties is helpful to better understand the mechanisms of ASB bone fracture.

The reason this haptic feedback is still poorly understood may be explained by the complex geometry presented by ASB bones (Figure 1), which are highly resistant to the use of conventional mechanical tests (bending, strain or torsion tests). Such tests require standardized geometrical samples of the material, impossible in this case due to these bones' anatomical properties. Furthermore, conventional tests do not take into account the variable microstructure that could be related to different mechanical behaviors.

Spherical depth-sensing indentation is an engineering technique involving pressing a hard-tipped material into another material with a known force, which has already been used to characterize the mechanical properties of human femoral cortical bone (Boughton *et al.*, 2018). The elastic modulus of a material is calculated from the loading (Hertz relation (Hertz, 1882)) or unloading curve (Oliver and Pharr theory (Oliver and Pharr, 2004)). The advantage of spherical rather than sharp-tip indentation is that, at small loads and displacements, the deformation is almost entirely elastic using the former (Oliver and Pharr, 2004). The viscoelastic behavior of biological materials can generate unloading curves that are difficult to interpret using the Oliver and Pharr method (Malgat *et al.*, 2016). In addition, the indentation in a liquid medium makes it difficult to detect the point of contact. This difficulty affects the results from the Oliver and Pharr method, but has no influence on the Hertz relationship (Jehl et al., 2016). To illustrate the impact of the analysis method, an experiment on a well-studied bone (femur cortical bone) is presented in supplementary material (Supplementary material S1). A finite element simulation confirms the validity of the developed method

(Supplementary material S2). Arnold and colleagues (Arnold *et al.*, 2017) conducted a systematic review on micro-indentation used to measure cortical bone stiffness. They concluded that "due to the porous nature of cortical bone at the millimeter scale, the apparent elastic modulus at the millimeter scale will be less than the modulus at a smaller material scale, where pores will not affect its stiffness" and recommended combining indentation with high-resolution imaging. In the study presented herein, a nanoindenter associated with micro-CT imaging were therefore used.

The reduced Young's moduli reported in this study are lower than data reported on other cortical bones. The method described here was not intended to provide explanations of such low moduli. However, several hypotheses can be drawn. First, in ASB cortical bones, the orientation of osteons/lamellae is poorly studied but seems to be randomly distributed (Dempster, 1967) (supplementary material S3) and may lead to different mechanical properties (Smit et al., 2002). It is radically different from long bones, where osteons are oriented along the loading force axis in long bone and vertebrae (Roy *et al.*, 1998). Second, the bone mineral density may be different in ASB bones, and will be study in further works. Finally, ASB bones have an embryological origin different from long bones: the former develop from the neural crest, the latter from the mesoderm (McBratney-Owen *et al.*, 2008). A flaw in the measurement method could also have been discussed, but this method was validated on a femur cortical bone (supplementary material S1) and found similar results than previous study using indentation tests (Boughton *et al.*, 2019). Nevertheless, it will be interesting to evaluate the impact of the liquid medium (saline solution) on the nanoindentation results, compared to other liquid medium (Hank's balanced saline solution, HBSS) (Habelitz et al., 2002).

To establish a measurement protocol, environmental parameters must be set to characterize the bone's behavior in a physiological way. Dehydration (Rodriguez-Florez *et al.*, 2013) and temperature are known to increase the stiffness and strength of cortical bone (Nyman *et al.*, 2006). An experimental design was thus created according to the L8 Taguchi orthogonal array (Taguchi, 1990)

fixing four parameters: **i)** temperature, **ii)** hydration, **iii)** loading curve fitting method, and **iv)** bone microstructure.

i) Our results demonstrate that the two temperature levels studied (20 and 37°C) had no impact on the mechanical properties of ASB bones (Figure 4). Furthermore, temperature had only a weak influence on the environment (Figure 5.C.). Similarly, while there was a slight difference in mechanical behavior when comparing the bone structures according to temperature, the effect of this interaction is related to measurement dispersion, and is not significant (Figure 5.B). Thus, to simplify the experimental protocol, we chose to perform future tests at ambient temperature (20°C).

ii) In contrast, the hydration status was found to be important, since the results demonstrate a reduced Young's modulus (E*) four times higher in the dry samples (Figure 4). In the human body, water resides within the bone canals and also within the extracellular mineralized matrix (Nyman *et al.*, 2006). We therefore chose to set a liquid environment to replicate the human bone physiology. Furthermore, interaction between bone and hydration status (Figure 5.A) revealed greater difference in the dry environment. We hypothesize that drying improves the difference between low and high-porosity bones in a non-physiological manner (denaturation).

iii) The Hertzian contact theory (Hertz, 1882) enabled us to study part (or all) of the loading curve of the nanoindentation tests (Figure 3). The mechanical characterization obtained by curve indentation fitting requires one to hand-select the contact point (beginning of the test) in order to overcome the bone roughness and complex geometric surfaces. This is why we chose to compare tests with the curve indentation fitting at the start (10% to 50% of the load) as well as at the end (50% to 98%) of the load, the latter not requiring human selection. Our results reveal a significant difference of 63 MPa for E* (Table 1). This can be explained by the residual soft tissues at the bone surface (periosteum). Curve indentation fitting at the end of the learning curve would appear to be the optimal solution to avoid interpretation bias.

iv) The results show the different mechanical properties presented by LPB compared to HPB (Figure 4). HPB cause reduced stiffness consistent with the literature (Cooper *et al.*, 2016). Thus, nanoindentation would appear a suitable technique for studying the mechanical behavior of these bones according to the variation of the internal microstructure.

To confirm the protocol based on these parameters, two new bone samples were scanned and tested. The results are summarized in Table 2. This protocol enables the differentiation of bone microstructures, using an environment close to physiological conditions. A thorough analysis and quantification of the microstructure via micro-CT will be performed in future experiments, which could explain the standard deviation values (Boruah *et al.*, 2017).

Characterization of specimen 2	**Reduced Young's Modulus E* (mean)**	**Reduced Young's Modulus E* (median)**	**Standard deviation E***	**Range**	**P-value (test)**
Low-porosity bone (10.8%)	994.68 MPa	991.94 MPa	342.52 MPa	434 to 1745.2 MPa	< 0.0001 (Welch's t-test)
High-porosity bone (60%)	409.79 MPa	379.07 MPa	175.14 MPa	206.09 to 755.56 MPa	

Table 3: Main results of characterization in protocol validation (specimen 2)

5. Conclusion

The aim of the study was to define the environment for ASB bones measurements. The choice of comparison from E*, associated with suitable measurement conditions (low load, low loading speed), represents a first step in the characterization of these bones.

Nanoindentation associated with micro-CT imaging would appear to be the optimal technique to characterize the mechanical properties of thin ASB bone walls, capable of differentiating between samples according to microstructure. Furthermore, to obtain the physiological properties of ASB, the tests must be performed involving immersion. Temperature during testing does not interfere with the mechanical properties, and future experiments should ideally be performed in 20°C temperature and a liquid (physiological saline sodium chloride) environment to measure ASB mechanical properties. Finally, it is recommended to perform curve fitting at the end of the load.

Future experiments will use the integrated Sinus Mode, which enables to perform Dynamic Mechanical Analysis for depth profiling of mechanical properties (HIT, EIT vs. depth) and measurement of viscoelastic properties (E', E'': storage and loss moduli, tan δ) on samples ranging. Viscoelastic indentation responses will be examined based on an approach using elastic–viscoelastic correspondence. These experiments will be coupled with a precise analysis of the microstructure (bone mineral density, porosity and orientation of the osteons) using micro-CT. Furthermore, other mechanical tests will be performed (uniaxial and biaxial microtraction) to study the anisotropy of ASB bones.

Acknowledgments

The authors wish to acknowledge the laboratory of anatomy of Nancy, France, for their valuable collaboration, Mrs Kathryn Atkins for the English editing, and the ASCATIM FEDER PROJECT (University of Lorraine) and CarMoSim startup company for their valuable participation and support.

Funding

This work was partially funded by the “Collège Français d’ORL et chirurgie cervico-faciale” (no grant number available).

References

Alexander SL, Rafaels K, Gunnarsson CA, Weerasooriya T. Structural analysis of the frontal and parietal bones of the human skull. Journal of the Mechanical Behavior of Biomedical Materials. 1 févr 2019;90:689-701. DOI: 10.1016/j.jmbbm.2018.10.035

Arnold M, Zhao S, Ma S, Giuliani F, Hansen U, Cobb JP, et al. Microindentation - a tool for measuring cortical bone stiffness? A systematic review. Bone Joint Res. 2017 Sep;6(9):542–9. DOI: 10.1302/2046-3758.69.BJR-2016-0317.R2

Bakhach J. The cryopreservation of composite tissues. Organogenesis. 2009;5(3):119–26. DOI: 10.4161/org.5.3.9583

Berger G, Eviatar E, Kogan T, Landsberg R. The normal uncinate process: histology and clinical relevance. Eur Arch Otorhinolaryngol. mars 2013;270(3):959-64. DOI: 10.1007/s00405-012-2169-2

Boruah S, Subit DL, Paskoff GR, Shender BS, Crandall JR, Salzar RS. Influence of bone microstructure on the mechanical properties of skull cortical bone - A combined experimental and computational approach. J Mech Behav Biomed Mater. 2017;65:688–704. DOI: 10.1016/j.jmbbm.2016.09.041

Boughton OR, Ma S, Zhao S, Arnold M, Lewis A, Hansen U, et al. Measuring bone stiffness using spherical indentation. PLOS ONE. 2018 Jul 12;13(7):e0200475. DOI: 10.1371/journal.pone.0200475

Boughton OR, Ma S, Cai X, Yan L, Peralta L, Laugier P, et al. Computed tomography porosity and spherical indentation for determining cortical bone millimetre-scale mechanical properties. Scientific Reports. 2019 May 15;9(1):1–15. DOI: 10.1038/s41598-019-43686-6

Bouxsein ML, Boyd SK, Christiansen BA, Guldberg RE, Jepsen KJ, Müller R. Guidelines for assessment of bone microstructure in rodents using micro–computed tomography. Journal of Bone and Mineral Research. 2010;25(7):1468–86.

Cooper DML, Kawalilak CE, Harrison K, Johnston BD, Johnston JD. Cortical Bone Porosity: What Is It, Why Is It Important, and How Can We Detect It? Curr Osteoporos Rep. 2016;14(5):187–98. DOI: 10.1007/s11914-016-0319-y

Dall'Ara E, Schmidt R, Zysset P. Microindentation can discriminate between damaged and intact human bone tissue. Bone. 2012 Apr;50(4):925–9. DOI: 10.1016/j.bone.2012.01.002

Dempster WT. Correlation of types of cortical grain structure with architectural features of the human skull. American Journal of Anatomy. 1967;120(1):7–31. DOI: 10.1002/aja.1001200103

Favier V, Zemiti N, Caravaca Mora O, Subsol G, Captier G, Lebrun R, et al. Geometric and mechanical evaluation of 3D-printing materials for skull base anatomical education and endoscopic surgery simulation - A first step to create reliable customized simulators. PLoS ONE. 2017;12(12):e0189486. DOI: 10.1371/journal.pone.0189486

Favier V, Gallet P, Subsol G, Captier G. Understanding the Biomechanical Properties of Skull Base Tissues Is Essential for the Future of Virtual Reality Endoscopic Sinus and Skull Base Surgery Simulators. Clin Exp Otorhinolaryngol. 2019;12(2):231-2. DOI: 10.21053/ceo.2018.01627

Fischer-Cripps AC. Study of analysis methods of depth-sensing indentation test data for spherical indenters. Journal of Materials Research. juin 2001;16(6):1579-84. DOI: 10.1557/JMR.2001.0219

Habelitz S, Marshall GW, Balooch M, Marshall SJ. Nanoindentation and storage of teeth. J Biomech. 2002 Jul;35(7):995–8. DOI: 10.1016/s0021-9290(02)00039-8

Hertz H. Ueber die Berührung fester elastischer Körper. Journal für die reine und angewandte Mathematik. 1882;92:156–71.

Hosemann W, Draf C. Danger points, complications and medico-legal aspects in endoscopic sinus surgery. GMS Curr Top Otorhinolaryngol Head Neck Surg. 2013 Dec 13;12:Doc06. DOI: 10.3205/cto000098

Jehl J, Pierson G, Voignier A, Kouitat Njiwa R. On the depth sensing indentation on liquid environment for application to biological tissue. In: Kongoli F, Kobe S, Calin M, Dong C, editors. Sustainable Industrial Processing Summit SIPS 2016 Volume 2: Dubois Intl. Symp. / Complex Metallic Systems. Volume 2. Montreal(Canada): FLOGEN Star Outreach. 2016. p. 94-95.

Lovie, P. Interaction Plot. In Encyclopedia of Statistics in Behavioral Science (eds B.S. Everitt and D.C. Howell). 2005. DOI: 10.1002/0470013192.bsa307

Lundstedt T, Seifert E, Abramo L, Thelin B, Nyström Å, Pettersen J, et al. Experimental design and optimization. Chemometrics and Intelligent Laboratory Systems. 24 août 1998;42(1):3-40. DOI: 10.1016/S0169-7439(98)00065-3

Malgat R, Faure F, Boudaoud A. A Mechanical Model to Interpret Cell-Scale Indentation Experiments on Plant Tissues in Terms of Cell Wall Elasticity and Turgor Pressure. Front Plant Sci. 2016;7:1351. DOI: 10.3389/fpls.2016.01351

McBratney-Owen B, Iseki S, Bamforth SD, Olsen BR, Morriss-Kay GM. Development and tissue origins of the mammalian cranial base. Dev Biol. 2008 Oct 1;322(1):121–32. DOI: 10.1016/j.ydbio.2008.07.016

Nyman JS, Roy A, Shen X, Acuna RL, Tyler JH, Wang X. The influence of water removal on the strength and toughness of cortical bone. J Biomech. 2006;39(5):931–8. DOI: 10.1016/j.jbiomech.2005.01.012

Oliver WC, Pharr GM. Measurement of hardness and elastic modulus by instrumented indentation: Advances in understanding and refinements to methodology. Journal of Materials Research. 2004 Jan;19(1):3–20. DOI: 10.1557/jmr.2004.19.1.3

Oyen ML, Shean TAV, Strange DGT, Galli M. Size effects in indentation of hydrated biological tissues. Journal of Materials Research. 2012 Jan;27(1):245–55. DOI: 10.1557/jmr.2011.322

Raul J-S, Deck C, Willinger R, Ludes B. Finite-element models of the human head and their applications in forensic practice. Int J Legal Med. sept 2008;122(5):359-66. DOI: 10.1007/s00414-008-0248-0

Rho J-Y, Tsui TY, Pharr GM. Elastic properties of human cortical and trabecular lamellar bone measured by nanoindentation. Biomaterials. 1997 Oct 1;18(20):1325–30. DOI: 10.1016/S0142-9612(97)00073-2

Rodriguez-Florez N, Oyen ML, Shefelbine SJ. Insight into differences in nanoindentation properties of bone. Journal of the Mechanical Behavior of Biomedical Materials. 2013 Feb 1;18:90–9. DOI: 10.1016/j.jmbbm.2012.11.005

Roy ME, Rho JY, Tsui TY, Evans ND, Pharr GM. Mechanical and morphological variation of the human lumbar vertebral cortical and trabecular bone. J Biomed Mater Res. 1999 Feb;44(2):191–7. DOI: 10.1002/(sici)1097-4636(199902)44:2<191::aid-jbm9>3.0.co;2-g

Smit TH, Huyghe JM, Cowin SC. Estimation of the poroelastic parameters of cortical bone. Journal of Biomechanics. 2002 Jun 1;35(6):829–35. DOI: 10.1016/S0021-9290(02)00021-0

Taguchi G. Introduction to Quality Engineering, Asian Productivity Organization, Tokyo, 1990.

Våpenstad C, Hofstad EF, Bø LE, Kuhry E, Johnsen G, Mårvik R, et al. Lack of transfer of skills after virtual reality simulator training with haptic feedback. Minim Invasive Ther Allied Technol. 2017 Dec;26(6):346–54. DOI: 10.1080/13645706.2017.1319866

Waridel F, Monnier P, Agrifoglio A. Evaluation of the bone resistance of the sphenoid and ethmoid sinuses. Laryngoscope. 1997 Dec;107(12 Pt 1):1667–70. DOI: 10.1097/00005537-199712000-00017

White PS, Nassif R, Saleh H, Drew T. Pilot study of a device for measuring instrument forces during endoscopic sinus surgery. Acta Otolaryngol. 2004 Mar;124(2):176–8. DOI: 10.1080/00016480410016568

Yamauchi Y, Yamashita J, Morikawa O, Hashimoto R, Mochimaru M, Fukui Y, et al. Surgical Skill Evaluation by Force Data for Endoscopic Sinus Surgery Training System. In: Dohi T, Kikinis R, editors. Medical Image Computing and Computer-Assisted Intervention — MICCAI 2002. Berlin, Heidelberg: Springer; 2002. p. 44–51. (Lecture Notes in Computer Science). DOI: 10.1007/3-540-45786-0_6

Skull base bone samples

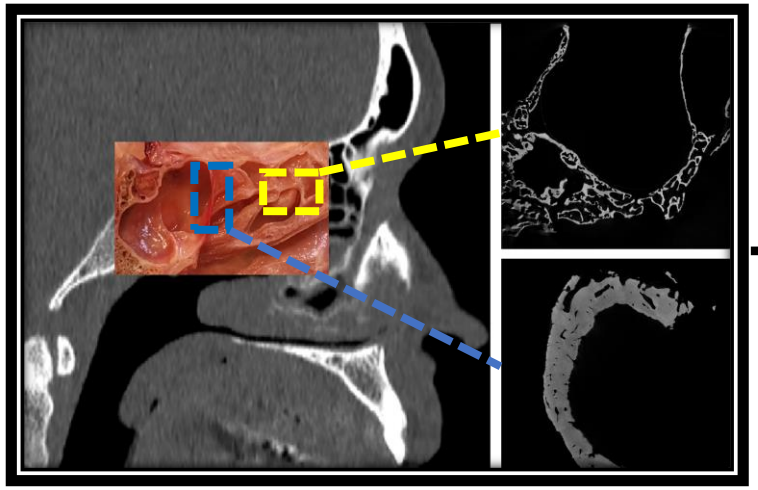

Nano-indentation experimental design

Tests	Bone microstructure	Hydration status	Temperature	Analysis
# 1	Low-Porosity	Dry	20°C	Start
# 2	Low-Porosity	Dry	37°C	End
# 3	Low-Porosity	Hydrated	20°C	End
# 4	Low-Porosity	Hydrated	37°C	Start
# 5	High-Porosity	Dry	20°C	End
# 6	High-Porosity	Dry	37°C	Start
# 7	High-Porosity	Hydrated	20°C	Start
# 8	High-Porosity	Hydrated	37°C	End

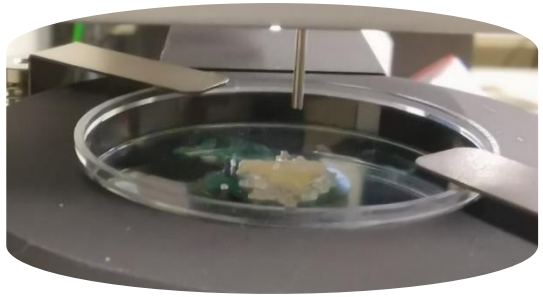

Temperature

Hydration status

Microstructure analysis

Loading curve fitting (Hertz)

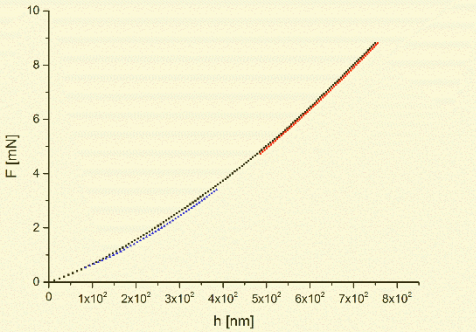

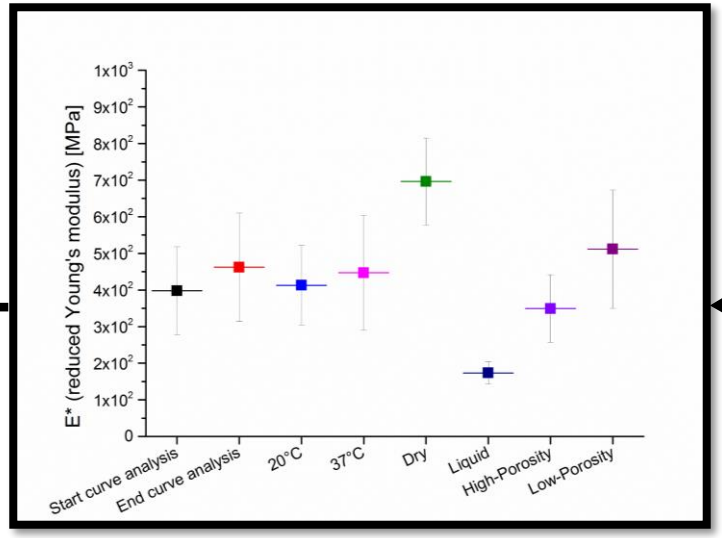

Final setting of parameters

- **Temperature: 20°C**
- **Environment: liquid**
- **Loading curve fitting: end**